

## Exchange bias between magnetoelectric $\text{YMnO}_3$ and ferromagnetic $\text{SrRuO}_3$ epitaxial films

X. Martí, F. Sánchez,<sup>a)</sup> and J. Fontcuberta

*Institut de Ciència de Materials de Barcelona, CSIC, Campus UAB, Bellaterra 08193, Spain*

M. V. García-Cuenca, C. Ferrater, and M. Varela

*Departament de Física Aplicada i Òptica, Universitat de Barcelona, Diagonal 647, Barcelona 08028, Spain*

(Presented on 2 November 2005; published online 20 April 2006)

Orthorhombic  $\text{YMnO}_3$  (YMO) epitaxial thin films were deposited on  $\text{SrTiO}_3$  (STO) single-crystal substrates. We show that the out-of-plane texture of the YMO films can be tailored using STO substrates having (001), (110), or (111) orientations. We report on the magnetic properties of the YMO(010) films grown on STO(001) substrates. The dependence of the susceptibility on the temperature indicates that the films are antiferromagnetic below the Néel temperature (around 35 K). Orthorhombic YMO(010) films were also deposited on an epitaxial buffer layer of ferromagnetic and metallic  $\text{SrRuO}_3$  (SRO). The magnetic hysteresis loops of SRO show exchange bias at temperatures below the Néel temperature of YMO. These results confirm that the YMO films are antiferromagnetic and demonstrate that magnetoelectric YMO can be integrated in functional epitaxial architectures. © 2006 American Institute of Physics. [DOI: 10.1063/1.2167333]

### INTRODUCTION

Multifunctional materials research is of fundamental importance for the next generation of devices of relevance in several areas of science and technology, including magneto-electronics. Biferroic materials show the coexistence of ferroelectricity and magnetic order and are currently receiving much attention (see two recent reviews in Refs. 1 and 2). One of the most studied materials is the hexagonal phase of  $\text{YMnO}_3$  (YMO), which is ferroelectric and antiferromagnetic (AF).<sup>3</sup> The orthorhombic phase of YMO is not ferroelectric, but substantial changes of the dielectric constant close to the AF order temperature have been reported.<sup>4</sup>

The orthorhombic phase of YMO is metastable in bulk, and it forms only when high pressures are applied<sup>4</sup> or by soft chemistry techniques.<sup>5,6</sup> YMO belongs to the family of  $\text{RMnO}_3$  compounds, where  $R$  is a trivalent cation. These compounds can present either hexagonal or orthorhombic structure, depending on the size of the  $R^{3+}$  cation.<sup>7</sup> Specific volume is lower in the perovskite (orthorhombic) phase than in the hexagonal, and the orthorhombic phase can be stabilized in bulk samples under high pressures. This phase can be also stabilized in YMO thin films under compressive epitaxial stress.<sup>8–10</sup> Whereas the phase stabilization is documented in these references, the physical properties of orthorhombic YMO films are not reported.

We report here on the growth and magnetic characterization of AF perovskite YMO thin films. Epitaxial films were deposited on  $\text{SrTiO}_3$  (STO) substrates having different orientations; we will show that this strategy allows selection of the YMO crystal out-of-plane orientation. This is of fundamental importance towards device design since it makes possible having films with precisely controlled magnetic, ferroelectric, or magnetoelectric axis orientation. We present

magnetic measurements of the films grown on STO(001), confirming their AF character below the Néel temperature,  $T_N \sim 35$  K. Moreover, we report also on the growth and magnetic characterization of bilayers with YMO and  $\text{SrRuO}_3$  (SRO), a ferromagnetic and metallic oxide below  $\sim 150$  K.

### EXPERIMENT

YMO thin films, about 150 nm in thickness, were grown on (001)-, (110)-, and (111)-oriented STO substrates by pulsed laser deposition using a KrF excimer laser (248 nm wavelength and 34 ns pulse duration) with a repetition rate of 10 Hz. The laser beam was focused to a fluence around  $2.5 \text{ J/cm}^2$ , on a stoichiometric target of YMO. The target was rotated during the ablation process to reduce nonuniform erosion. The substrate was placed parallel to the target at a distance of 5 cm. The films were deposited at substrate temperatures of  $800^\circ\text{C}$ , under 0.15 mbar of oxygen. When the laser was switched off, the substrate was cooled down and 1 atm of oxygen was introduced at  $500^\circ\text{C}$ . A YMO/SRO bilayer was fabricated on a STO(001) substrate in a single-step process, SRO being the bottom layer. The crystal structure and lattice parameters were investigated by x-ray diffraction (XRD) using  $\text{Cu } K_\alpha$  radiation. The magnetic properties of YMO films on STO(001) and YMO/SRO bilayers on STO(001) were measured by using a superconducting quantum interference device (SQUID) system, from 5 to 300 K and under field up to 5 T.

### RESULTS AND DISCUSSION

Figure 1 shows the XRD  $\theta/2\theta$  scans of YMO films on (a) STO(111), (b) STO(110), and (c) STO(001) substrates. The diffraction peaks correspond to reflections from the substrates or the orthorhombic phase of YMO. There are no reflections corresponding to the hexagonal phase. Each film has a single out-of-plane orientation, which depends on the

<sup>a)</sup>Electronic mail: fsanchez@icmab.es

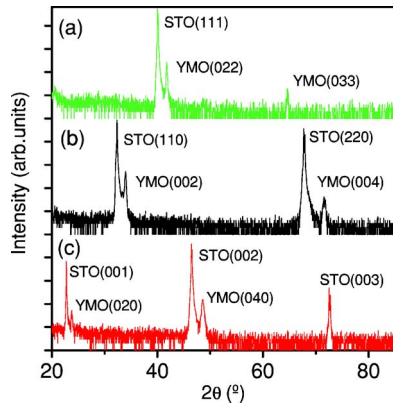


FIG. 1. XRD  $\theta/2\theta$  scans (intensity, in a.u., is plotted in a logarithmic scale) of YMO films on STO substrates: (a) (111), (b) (110), and (c) (001) oriented. Scans are vertically shifted for clarity.  $Pnma$  indexation is used for YMO peaks. The scans reveal that YMO films are orthorhombic, without traces of other phases, and with out-of-plane orientation that depends on the substrate orientation.

used substrate. Using the  $Pnma$  indexation ( $a=5.84 \text{ \AA}$ ,  $b=7.36 \text{ \AA}$ , and  $c=5.26 \text{ \AA}$ ) of orthorhombic bulk YMO, the orientation relationships are YMO(011)/STO(111), YMO(001)/STO(110), and YMO(010)/STO(001). The full width at half maximum of the rocking curves ( $\omega$  scans) of the out-of-plane reflections was around  $0.25^\circ$  in all cases.  $\phi$  scans (not shown) indicated that YMO films are epitaxial. From the position of the diffraction peaks in the  $\theta/2\theta$  scans, the out-of-plane lattice parameters of the three films were determined. The out-of-plane parameters are 4.31, 5.27, and  $7.45 \text{ \AA}$ , increasing with respect to the bulk phase by 0.5%, 0.1%, and 1.4% for films on STO(111), STO(110), and STO(001), respectively. It is to be noted that the increase in the out-of-plane parameter is consistent with an in-plane compressive stress. The stress is due to the epitaxial growth, which caused the stabilization of the orthorhombic phase.

We turn now to the magnetic properties of the YMO(010)/STO(001) samples. According to neutron-diffraction data<sup>6</sup> in the AF state of the orthorhombic YMO, the magnetic moments of  $\text{Mn}^{3+}$  ions lie in the  $a$ - $c$  crystal plane. Therefore, in our YMO(010)/STO(001) sample, with the  $b$  axis perpendicular to the film surface (as shown in Fig. 1), the atomic spins are located in the film plane. The magnetic susceptibility  $\chi$  was determined as a function of the temperature and with the magnetic field applied parallel to

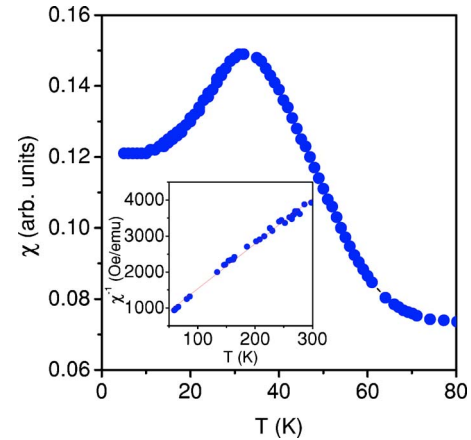


FIG. 2. Temperature dependence of the magnetic susceptibility (in a.u.) of a 150-nm-thick YMO film on STO(001). Magnetic field was set to 50 Oe and it was applied parallel to the plane of the sample. Inset: high-temperature dependence of the reciprocal of the susceptibility (measured with a 6 T field applied parallel to the plane of the sample).

the plane of the sample (Fig. 2). As expected,  $\chi(T)$  rises when lowering the temperature; a peak in  $\chi(T)$  signals the onset of AF ordering at the Néel temperature  $T_N \sim 35 \text{ K}$ . We note that this value of  $T_N$  is close to that reported ( $T_N \sim 42 \text{ K}$ ) for bulk samples.<sup>4,6</sup> We have also analyzed the susceptibility data in the paramagnetic region. In Fig. 2 (inset), where we show the reciprocal of the susceptibility plotted as a function of the temperature, it can be appreciated that the susceptibility displays a Curie-Weiss behavior. From these data, we extract an extrapolated Curie of about  $-25 \text{ K}$  and an effective paramagnetic moment  $\mu_{\text{eff}} \approx 5.14 \mu_B/\text{f.u.}$  We note that  $\mu_{\text{eff}} = 4.90 \mu_B$  is expected for a  $\text{Mn}^{3+}$  ion, which is very close to the estimated value; the difference is likely due to some unavoidable inaccuracy on the evaluation of film thickness and substrate subtraction of the magnetic data.

We have also prepared bilayers composed by the AF YMO and the ferromagnetic SRO. SRO has a structure of distorted perovskite, with a pseudocubic lattice parameter very close to that of STO (lattice mismatch is  $\sim 0.6\%$ ) and it can be grown epitaxially on STO.<sup>11</sup> XRD characterization (not shown here) indicates that YMO films grown on SRO/STO(001) are orthorhombic and (010) oriented, as they are when grown directly on the STO(001) substrate. We measured the hysteresis loops with the magnetic field applied

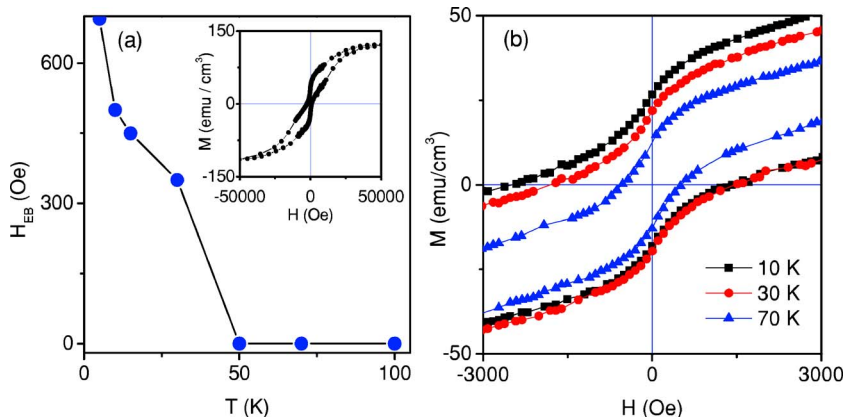


FIG. 3. Exchange bias in YMO/SRO bilayers: (a) exchange bias field plotted against the temperature. The dependence indicates that the YMO layer is antiferromagnetic below  $T_N \sim 35 \text{ K}$ . The inset shows a hysteresis loop at  $T=5 \text{ K}$  measured by applying field parallel to the plane of the sample. (b) Detail (low-field dependence) of hysteresis loops at 10 K (squares), 30 K (circles), and 70 K (triangles). Note that at the lowest temperatures there is a clear shift of the center of the hysteresis loop due to the exchange bias coupling between both layers.

parallel to the plane of the sample. Spins in the AF layer lay in this plane, and an exchange bias field<sup>12</sup> ( $H_{\text{EB}}$ ) in the loops could be observed below the Néel temperature of YMO. In Fig. 3(a) (inset) we show a hysteresis loop measured at 10 K, after a field-cooling process from a temperature well above  $T_N$ . Similar measurements were done at several temperatures; a zoom of the low-field region of the corresponding magnetization loops is included in Fig. 3(b). It is clear from this figure the presence of an exchange bias that increases when reducing the temperature. In Fig. 3(a) (main panel) we display the temperature dependence of the exchange bias field,  $H_{\text{EB}} = (H_{c1} + H_{c2})/2$ , where  $H_{c1}$  and  $H_{c2}$  are the crossing fields in both magnetization branches. Data in this figure indicate that the  $H_{\text{EB}}$  vanishes at some temperature in the 30–50 K range and thus, in agreement with the measurements (Fig. 2) performed on single YMO films, we infer that the antiferromagnetic transition occurs between 30 and 50 K.

## SUMMARY

In summary, films of orthorhombic YMO oxide were epitaxially grown with an out-of-plane orientation that can be tuned by an appropriate choice of the substrate. The magnetic properties of YMO(010) films were studied. The Néel temperature is determined to be around 35 K. YMO(010) films were also grown on ferromagnetic SRO layers, and a well-defined exchange bias field is observed below the Néel temperature of YMO. The selection of texture of YMO films

and the demonstration of the occurrence of an exchange bias between a ferromagnetic oxide and the magnetoelectric YMO could be also useful towards future applications.

## ACKNOWLEDGMENTS

Financial support by the MEC of the Spanish Government (Project Nos. NAN2004-9094-C03 and MAT2005-5656-C04) and FEDER is acknowledged.

<sup>1</sup>W. Prellier, M. P. Singh, and P. Murugavel, *J. Phys.: Condens. Matter* **17**, R803 (2005).

<sup>2</sup>M. Fiebig, *J. Phys. D* **38**, R123 (2005).

<sup>3</sup>B. B. van Aken, T. T. M. Palstra, A. Filippetti, and N. A. Spaldin, *Nat. Mater.* **3**, 164 (2004).

<sup>4</sup>B. Lorenz, Y. Q. Wang, Y. Y. Sun, and C. W. Chu, *Phys. Rev. B* **70**, 212412 (2004).

<sup>5</sup>H. W. Brinks, H. Fjellvag, and A. Kjekshus, *J. Solid State Chem.* **129**, 334 (1997).

<sup>6</sup>A. Muñoz, J. A. Alonso, M. T. Casáis, M. J. Martínez-Lope, J. L. Martínez, and M. T. Fernández-Díaz, *J. Phys.: Condens. Matter* **14**, 3285 (2002).

<sup>7</sup>I. E. Graboy, A. A. Bosak, O. Yu. Gorbenko, A. R. Kaul, C. Dubourdieu, J. P. Sénateur, V. L. Svetchnikov, and H. W. Zandbergen, *Chem. Mater.* **15**, 2632 (2003).

<sup>8</sup>P. A. Salvador, T. D. Doan, B. Mercey, and B. Raveau, *Chem. Mater.* **10**, 2592 (1998).

<sup>9</sup>A. A. Bosak *et al.*, *Thin Solid Films* **400**, 149 (2001).

<sup>10</sup>J. Dho, C. W. Leung, J. L. MacManus-Driscoll, and M. G. Blamire, *J. Cryst. Growth* **267**, 548 (2004).

<sup>11</sup>G. Herranz *et al.*, *Phys. Rev. B* **71**, 174411 (2005).

<sup>12</sup>J. Nogués and I. K. Schuller, *J. Magn. Magn. Mater.* **192**, 203 (1999).